




RESEARCH ARTICLE

Sensitivity of a simple atmospheric model to changing surface friction with implications for seasonal prediction

Wolfgang Wicker¹  | Richard J. Greatbatch^{1,2}  | Martin Claus^{1,2} 

¹Ocean Circulation and Climate Dynamics, GEOMAR Helmholtz Centre for Ocean Research, Kiel, Germany

²Faculty of Mathematics and Natural Sciences, Christian Albrechts Universität, Kiel, Germany

Correspondence

R. J. Greatbatch, GEOMAR Helmholtz Centre for Ocean Research, Düsternbrooker Weg 20, 24105 Kiel, Germany
Email: rgreatbatch@geomar.de

Abstract

An ensemble of idealized experiments with the simplified general circulation model PUMA is used to analyze the response to reduced surface friction, that is a strengthening of the eddy-driven jet, a weakening of the Eulerian mean overturning, and a suppression of baroclinic instability. The suppression of baroclinic instability is caused by an effect called the barotropic governor by which increased horizontal shear restricts the ability of baroclinic disturbances to convert available potential energy into kinetic energy. This governor effect ensures that the residual circulation and Eliassen–Palm flux (EP flux) divergence are largely invariant to the surface friction parameter despite the connection between surface friction, the Eulerian mean overturning, and the eddy-momentum flux. The suppression of instability leads to an increase in persistence measured by the period of peak variance on synoptic time-scales and a strengthened signal-to-noise ratio on seasonal time-scales. These findings suggest that the signal-to-noise paradox seen in the context of seasonal prediction can be caused by excess mechanical damping in atmospheric prediction systems inhibiting the barotropic governor effect.

KEYWORDS

atmosphere, barotropic governor, persistence, PUMA, signal-to-noise paradox, surface friction

1 | INTRODUCTION

Since the pioneering work by Eady (1949) and Charney (1947), baroclinic instability is regarded as the primary mechanism for extratropical variability on synoptic time-scales and has been studied intensively (e.g., Simmons and Hoskins, 1978; James, 1987). It plays an important role in the atmospheric energy budget converting available potential energy into eddy kinetic energy and subsequently zonal mean kinetic energy

during the growth and decay of baroclinic waves (Lorenz, 1955; Simmons and Hoskins, 1978). Moreover, both simple models and observations show that high-frequency perturbations produce low-frequency variability by nonlinear interaction (e.g., James and James, 1989; Cai and van den Dool, 1991; Lorenz and Hartmann, 2003). Understanding the mechanisms that control baroclinic instability is therefore important for applications from sub-seasonal to seasonal and decadal prediction.

After 1950, both quasi-geostrophic theory and numerical primitive equation models facilitated the analysis of how background flow characteristics influence baroclinic instability. Simmons and Hoskins (1980), for instance, found sensitivity of the baroclinic wave life cycle to the barotropic flow in a primitive equation model. James and Gray (1986) investigated the effect of surface friction on the energy budget of the atmosphere in a similar model. Surprisingly, they found that lowered surface drag reduces eddy kinetic energy by suppressing the conversion of potential energy due to increased horizontal shear by means of what they called the *barotropic governor*. The underlying mechanism can be explained with the aid of a simple two-layer quasi-geostrophic model (James, 1987) where, with increased horizontal shear, the meridional extent of baroclinic disturbances is restricted, limiting their ability to extract potential energy from the vertically sheared flow.

The present paper is motivated by the possible relevance of the barotropic governor to the so-called *signal-to-noise paradox* (Eade *et al.*, 2014; Scaife *et al.*, 2014; Dunstone *et al.*, 2016; Scaife and Smith, 2018) which has emerged in the context of seasonal and decadal prediction. Scaife *et al.* (2014) have shown remarkable success at forecasting the European winter climate and, in particular, the winter North Atlantic Oscillation (NAO) index, using a dynamical seasonal prediction model system initialized at the beginning of November. Although the ensemble mean is significantly correlated with the observations, the amplitude is much smaller, resulting in a small signal-to-noise ratio. Since this was pointed out, a number of statistical models have been tested in order to explain the signal-to-noise paradox (Siegert *et al.*, 2016; Strommen and Palmer, 2019; Zhang and Kirtman, 2019). These statistical models indicate a possible misrepresentation of internal noise and anomaly persistence in dynamical atmospheric models. Specifically, Strommen and Palmer (2019) suggest that seasonal and decadal prediction models might contain excess stochasticity. Rapid growth of perturbations by baroclinic instability poses a reasonable first guess for the origin of that stochasticity. The consequent hypothesis that mistuned mechanical damping and a suppressing of the governor effect affect persistence and the signal-to-noise ratio provides the motivation for this study.

Here, idealized experiments are conducted with a simplified atmospheric general circulation model to analyze the impact of the barotropic governor by varying surface friction. The dry-dynamical core model with simplified physics is chosen to draw a clear picture of the dynamical consequences without the complication of transient forcing or complex parametrizations and to produce statistically robust results with long model simulations at a

low computational cost. Section 2 introduces the experimental set-up and describes all components necessary to study the barotropic governor and its effects on variability. In Section 3.1 it is confirmed that reducing surface friction suppresses baroclinic instability and new light is shed on the dynamical consequences. Evidence that the suppression of instability increases the synoptic eddy time-scale and can consequently lead to larger signal-to-noise ratios in seasonal forecasts is shown in Section 3.2. Finally, the general concept of a governor for instability and its implications for sophisticated climate models is discussed in Section 4.

2 | MODEL SET-UP

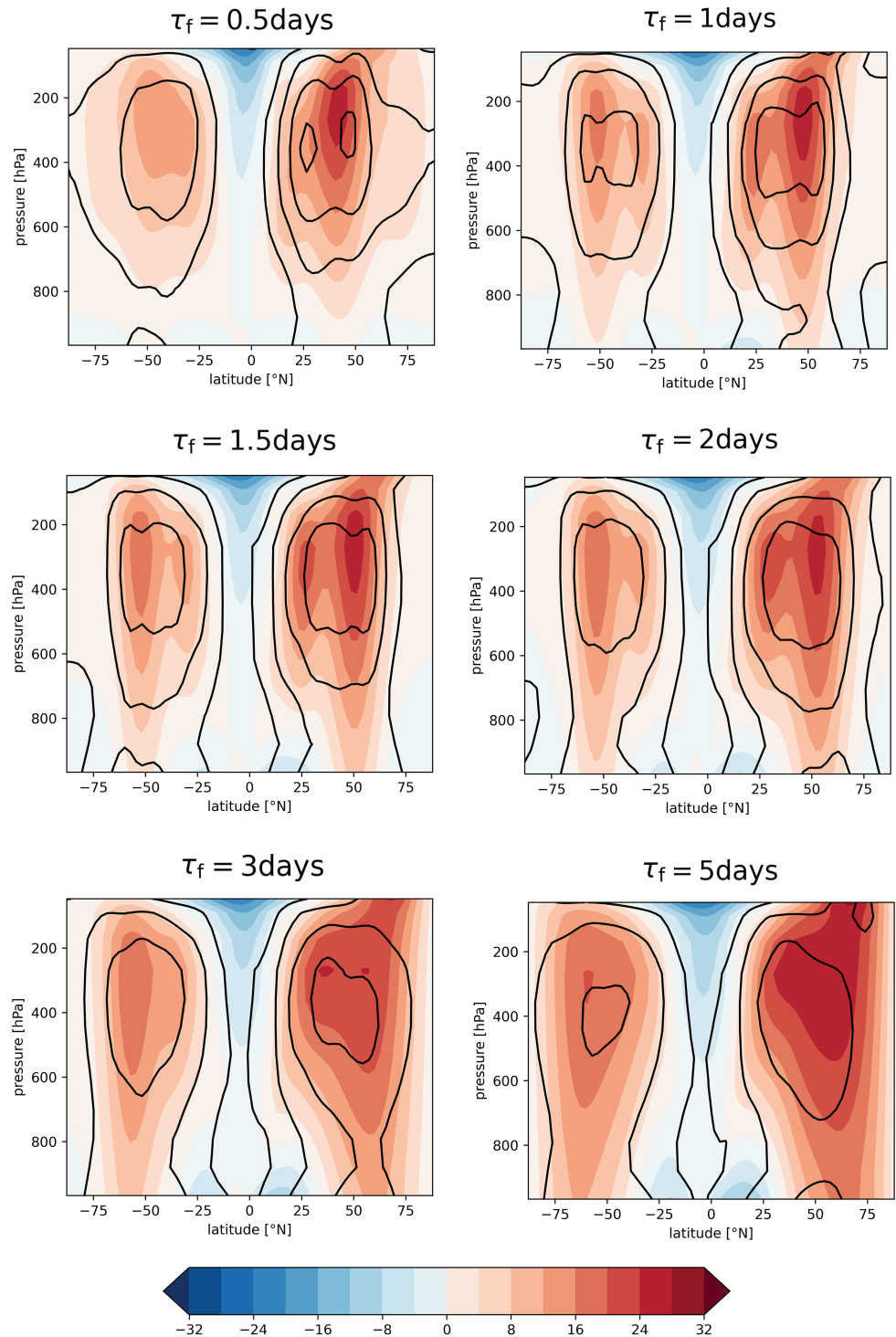
This study uses the Portable University Model of the Atmosphere (PUMA; Fraedrich *et al.*, 1998, 2005) which is a simple global circulation model based on the multi-layer spectral model of Hoskins and Simmons (1975) with dry dynamics and simplified parametrizations. The same model core was used by James and Gray (1986) when they discovered the governor effect. It integrates the hydrostatic primitive equations on a sphere in σ -coordinates where σ is pressure divided by surface pressure. In the set-up employed here, the model has been used to analyze jet dynamics and extratropical variability with a focus on the relationship between wave breaking and the NAO (Kunz *et al.*, 2009).

Specifically, we first use the model in an aquaplanet configuration with zonally symmetric boundary conditions. The spectral resolution of T42 is equivalent to a shortest resolvable length-scale of 152 km and is sufficient to capture baroclinic instability and barotropic Rossby waves. Following Scinocca and Haynes (1998), the model has 30 vertical levels that include nine levels in the troposphere and a sponge layer in the middle atmosphere to remove artifacts induced by the upper boundary condition. The surface influence on horizontal momentum within the planetary boundary layer is parametrized by linear Rayleigh friction given by:

$$\frac{\partial U}{\partial t} \sim -\frac{1}{\tau_f \frac{0.3}{\sigma-0.7}} U; \quad 0.7 < \sigma \leq 1. \quad (1)$$

The strength of friction reduces linearly from its maximum at the surface to zero at roughly 700 hPa. Non-zero friction is applied only at the three lowermost levels. To analyze the influence of the barotropic governor, the surface friction time-scale τ_f is varied between 0.5 and 5 days. A short time-scale corresponds to strong friction. Note that an aquaplanet set-up, as used here, without orography removing momentum from the zonal flow, might

FIGURE 1 Time-mean zonal-mean zonal wind (colour shading; $\text{m}\cdot\text{s}^{-1}$); black contours (spacing $2\text{ m}\cdot\text{s}^{-1}$) indicate the standard deviation using the departure from that mean at every gridpoint



require a larger friction coefficient than a model with a more realistic surface boundary.

Differential diabatic heating, parametrized by Newtonian temperature relaxation, is the source of midlatitude baroclinicity in this model. The setting is fixed to perpetual boreal winter conditions. At the surface, the zonally symmetric restoration temperature field is based on an Equator to winter pole difference of 70 K and an Equator to summer pole difference of 50 K. In the vertical,

it follows the vertical temperature gradient of the U.S. Standard Atmosphere with a reversed meridional temperature gradient in the lower stratosphere. Above, the restoration temperature field is set to produce a stratospheric polar vortex of medium strength (Kunz *et al.*, 2009, their Figure 1e,f). The relaxation time-scale increases gradually with height from five days at the lowest level to 40 days in the mid-upper troposphere and above (Kunz *et al.*, 2009). Furthermore, note that, since the model is

dry, there is no latent heat release by moist convection. To close the turbulent cascade at small scales, hyperdiffusion is applied to both momentum and temperature.

This simple experimental set-up provides a basis to analyze the barotropic governor without stationary waves excited by land–sea heating contrasts or orography, and without the complication of a seasonal cycle. The ensemble of experiments consists of 255 year-long simulations for each friction parameter where a spin-up phase of five years is excluded. These long simulations, equivalent to 1,000 consecutive winters for each experiment, allow us to draw statistically robust conclusions. The model output comprises daily snapshots of horizontal and vertical velocity, temperature, and geopotential height on pressure levels between 47 and 967 hPa which correspond to the twelve lowermost full model levels.

Our motivation is to investigate the possible importance of the barotropic governor for explaining the signal-to-noise paradox seen in seasonal predictions. Due to the chaotic nature of atmospheric dynamics, inherent predictability arising from initial conditions is generally limited to a few weeks (Lorenz, 1963; Smith *et al.*, 2012), but with some exceptions, e.g., O'Reilly *et al.* (2019). On the other hand, various seasonal prediction studies have shown that tropical precipitation anomalies, often controlled by atmosphere–ocean interaction, are an important source to seasonal prediction skill in the Extratropics (e.g., Scaife *et al.*, 2017; Wulff *et al.*, 2017; O'Reilly *et al.*, 2018; Hardiman *et al.*, 2020). Teleconnections associated with the El Niño–Southern Oscillation (ENSO) are among the most prominent examples for such a predictable signal (e.g., Horel and Wallace, 1981; Latif *et al.*, 1998). This study considers a scenario where all predictability arises from a stationary wave train caused by a tropical diabatic heating anomaly, and a long model run with constant boundary conditions is regarded as an ensemble of seasonal forecasts. Therefore, the experiments outlined above are repeated with a modified restoration temperature field which applies a diabatic heating anomaly following the approach by Gollan *et al.* (2019). Comparing the ensemble-mean and ensemble-spread response to changing surface friction enables deductions about the signal-to-noise ratio.

Gollan *et al.* (2019) make use of PUMA to investigate the influence of a stationary Rossby wave train produced by a localized heating anomaly on atmospheric blocking in the Extratropics. The three-dimensionally Gaussian-shaped anomaly with an amplitude of $1.5 \text{ K}\cdot\text{day}^{-1}$ centred in the equatorial mid-troposphere is designed to be weak El Niño-like, although, in contrast to realistic El Niño, the anomaly does not form a dipole and the longitudinal position is arbitrary in an otherwise

zonally symmetric set-up. For the analysis of variability on seasonal time-scales, the time series is grouped into alternating 90-day means and split into two independent ensembles. Differences between the two independent ensembles give an indication of statistical uncertainty. Again, we performed 255 year-long simulations for each parameter setting. With the partition into two independent ensembles outlined above, that makes an ensemble size of 500 members for each ensemble and each friction parameter. At this ensemble size, the ensemble mean has converged satisfactorily.

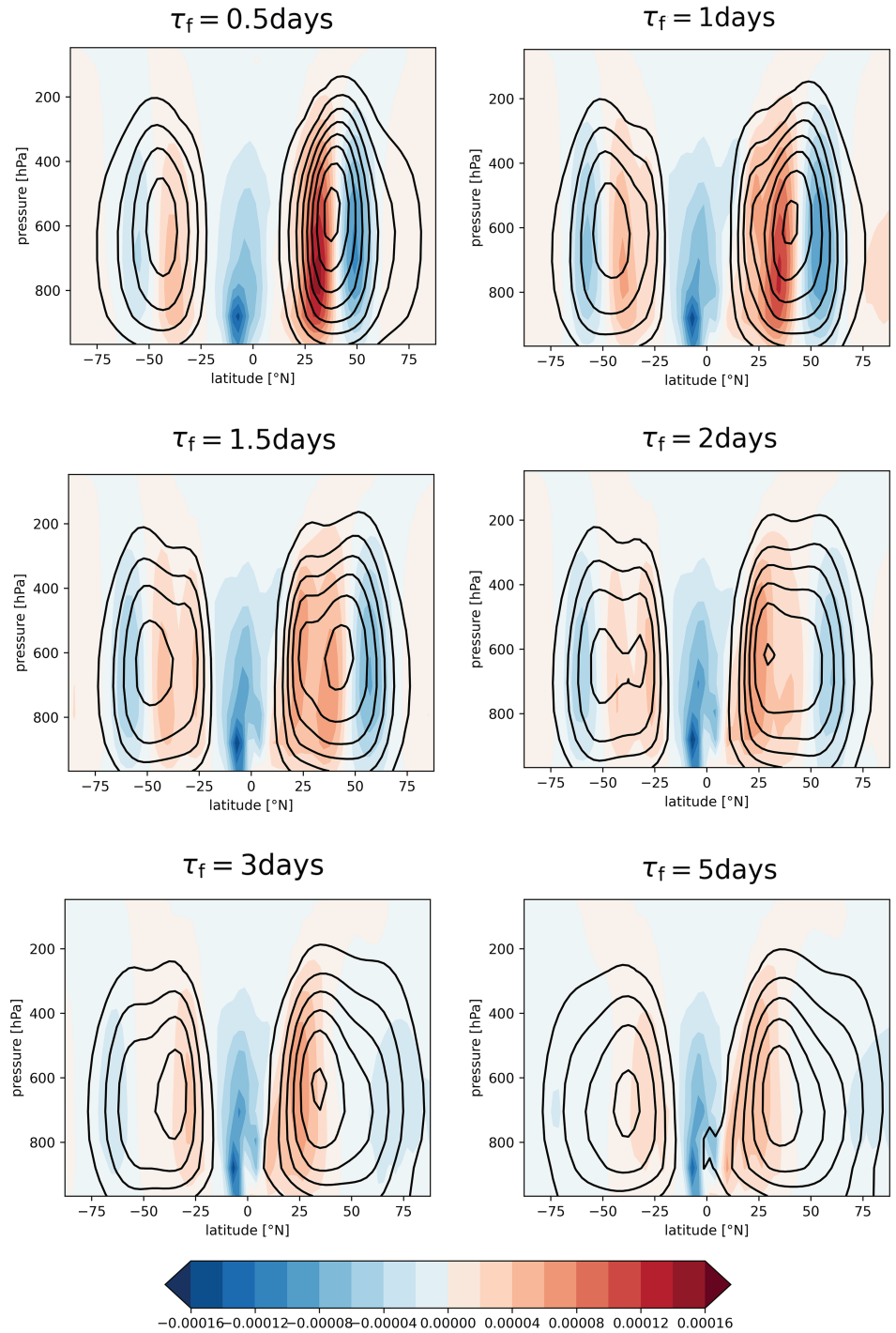
3 | MODEL RESULTS

3.1 | Suppression of baroclinic instability and a poleward shift of the storm track

In the temporal and zonal mean perspective, the westerly flow in the aquaplanet simulations is dominated by the characteristic jet structure with a baroclinic subtropical jet and a more barotropic eddy-driven jet further poleward in both hemispheres (Figure 1). For the strong friction cases ($1 \text{ day} \leq \tau_f \leq 2 \text{ days}$), these two westerly maxima are well separated, maximizing around 300 hPa at a zonal velocity of approximately $25 \text{ m}\cdot\text{s}^{-1}$. In contrast to the subtropical jet, since it reaches down to the surface, the eddy-driven jet is subject to linear friction. Consequently, the jet's barotropic component strengthens as the model's surface friction time-scale τ_f is increased. In addition to the strengthening, a poleward extension and a merging of jets can be seen at $\tau_f = 3 \text{ days}$. These results correspond well with the findings of previous studies (Stephenson, 1994; Robinson, 1997; Chen *et al.*, 2007) and increase confidence in the present model experiments. On the other hand, there are mean state biases that deserve mentioning. Equatorial winds are unrealistically easterly throughout the troposphere and the midlatitude jets' baroclinic components are too weak compared to reanalysis (not shown). It is not clear to what extent these biases can be attributed to the aquaplanet set-up or the absence of parametrized physics, especially moisture. Nevertheless, when the isolated tropical heating anomaly is added, as described in Section 2, the experiments show equatorial upper-tropospheric westerlies and a strengthened subtropical jet (not shown).

A first indication of the barotropic governor, as outlined in the Introduction, can be taken from the response of zonal wind variance to an increasing friction time-scale τ_f . Indicated by the black contours in Figure 1, the mean jets are associated with a significant amount of variance resulting from the instability of the mean flow. The maximum standard deviation lies above $8 \text{ m}\cdot\text{s}^{-1}$ for $\tau_f = 1 \text{ day}$.

FIGURE 2 As Figure 1, but for vertical velocity ($\text{Pa}\cdot\text{s}^{-1}$) with a contour spacing of $0.0001 \text{ Pa}\cdot\text{s}^{-1}$



Counterintuitively, but consistent with the barotropic governor, that measure shrinks as surface friction is reduced.¹

¹The standard deviation displayed in Figure 1 includes variations by zonally symmetric transients, transient eddies, and stationary eddies, although the latter reduce to zero on an aquaplanet for a sufficiently long temporal average. Strictly speaking, the barotropic governor affects baroclinic waves, that is, transient eddies, whereas annular mode-like variability is subject to a dynamical feedback between eddies and the mean. Supporting Information Figures S1, S2, and S3 show a

Further insight can be gained from the time-mean, zonal-mean vertical velocity shown in Figure 2, revealing the overturning cells associated with the Eulerian mean circulation. Note that these plots show vertical velocity in pressure coordinates where negative values indicate ascending air. Relating the characteristics of zonal-mean

decomposition of time-mean variance of zonal, vertical and meridional velocity into contributions by the zonally averaged circulation and the eddy part of the flow.

zonal momentum to the Eulerian mean overturning can be instructive. Namely, it is the subtropical jet that forms the poleward edge of the thermally direct Hadley cell, whereas the eddy-driven jet is co-located with the thermally indirect Ferrel cell. Poleward to that, we find a relatively weak thermally direct polar cell. The pole-to-pole asymmetry in December–February conditions can be seen in the shift of tropical ascent, with negative vertical velocities south of the Equator and a much stronger boreal Ferrel cell. Besides that, the standard deviation of daily data vertical velocity is concentrated at the Ferrel cell in the winter hemisphere. In general, the meridional overturning is too weak when compared to reanalysis (not shown) and the upper-tropospheric convective outflow at the Equator lies at too low a level (e.g., Karoly *et al.*, 1997 gives an observational estimate of the overturning circulation).

Interestingly, the PUMA model shows the strongest overturning for friction time-scales τ_f between 0.5 and 1.0 day (Figure 2). For an increasing friction time-scale τ_f , both the mean overturning and the standard deviation of vertical velocity reduces significantly as discussed later. Furthermore, it can be observed that, in the transition of the surface friction time-scale τ_f between 2 and 3 days, the thermally direct cell close to the pole disappears and the thermally indirect Ferrel cell extends to the pole.

So far, the reduction in the overall variance of zonal momentum and vertical velocity are the first signs of the barotropic governor. Additional evidence for a model response to changing surface friction, as reported by James and Gray (1986), can be gained by filtering synoptic-scale variance and plotting the model's storm track (Figure 3). Specifically, this is the zonal average of 2–7 day bandpass filtered variance of meridional velocity. Note that Figure 3 shows the storm track at 357 hPa. However, the general picture is similar throughout the middle and upper troposphere. The only difference of note is that the storm track is much broader at the surface. In Figure 3, it can be seen how the maximum strength of the storm track continuously declines in the Northern Hemisphere with increasing τ_f , consistent with the governor inhibiting baroclinic instability as the surface friction is reduced. In the Southern Hemisphere, there is an increase in the maximum variance from $\tau_f = 0.5$ day to 1 day, followed by a continual decline. Another prominent feature of Figure 3 is the poleward shift of peak variance as the surface friction is reduced, while the poleward boundary of the storm track remains relatively fixed for $\tau_f < 3$ days.

The poleward movement of the storm track is intriguing and possibly important to understand how the governor mechanism is represented in PUMA. The strengthening of the barotropic jet seen in Figure 1 increases the horizontal shear experienced by any disturbance from the zonal-mean flow. In the quasi-geostrophic

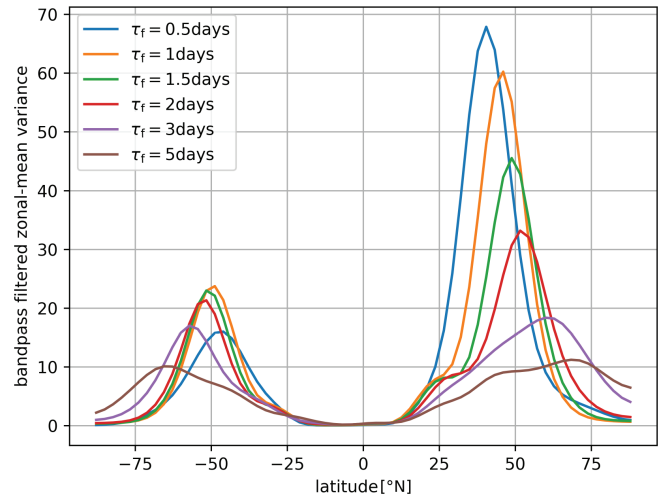
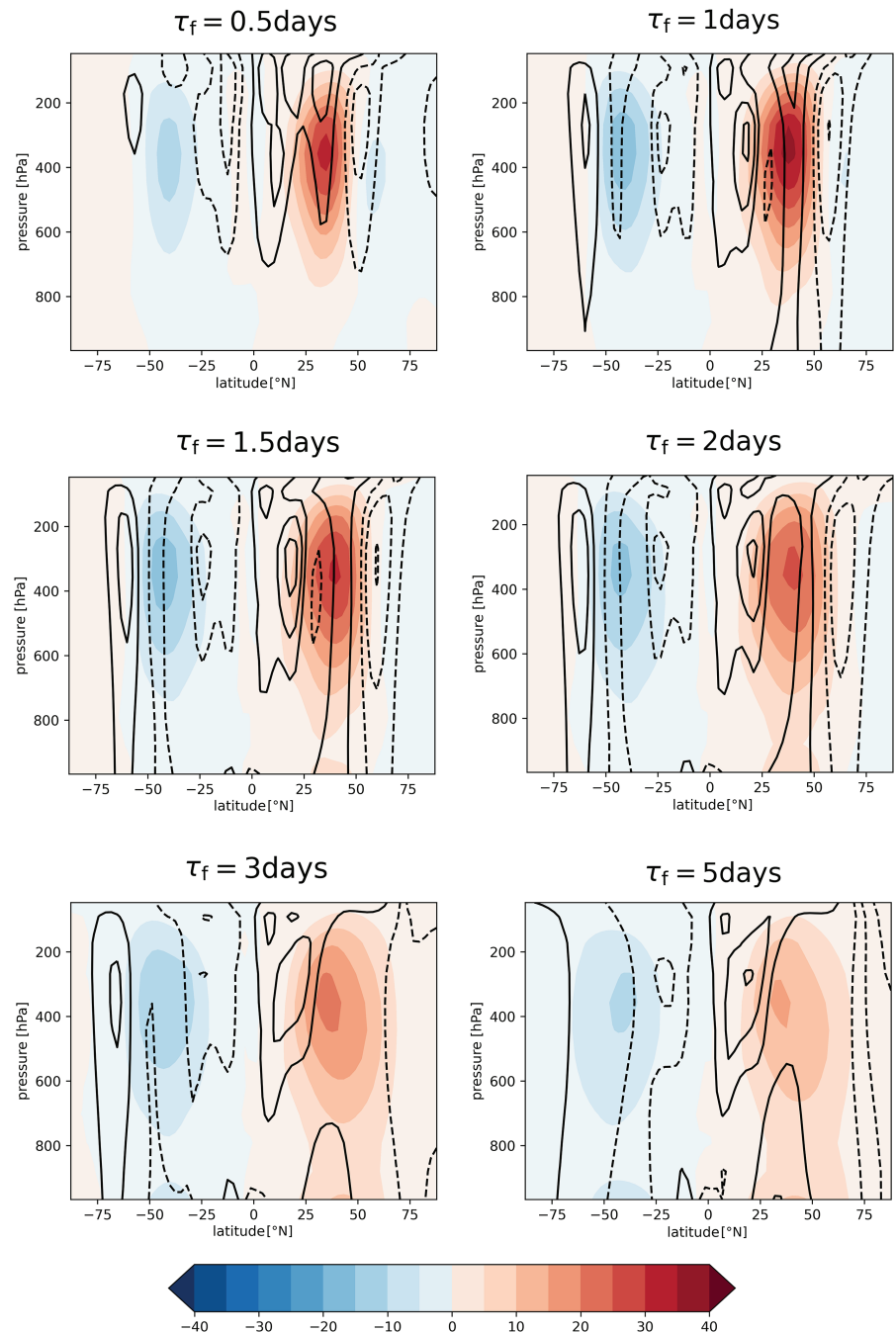


FIGURE 3 Zonal mean variance ($\text{m}^2 \cdot \text{s}^{-2}$) of 2–7 day bandpass filtered meridional velocity at 357 hPa for different aquaplanet configurations

model of James (1987), the shear acts to restrict the meridional extent of baroclinic disturbances, limiting their ability to convert available potential energy (APE) into eddy-kinetic energy (EKE). In our model, the response to increased shear is, apparently, a shift to higher latitudes away from the area of maximum baroclinicity. It has to be noted that the meridional temperature gradient is largely insensitive to changing the surface friction parameter (not shown), consistent with Robinson (1997). In addition to the meridional position or extent, James (1987) reports a vertical confinement of baroclinic disturbances to lower levels in response to increased Rossby wave dispersion. Something similar is observed in this study. Specifically, the storm track suppression in the upper troposphere (Figure 3) is stronger than at mid-tropospheric levels (not shown). Next to the ability to convert APE into EKE, growth rates of baroclinic disturbances can be offset by barotropic conversion due to Rossby wave dispersion (e.g., Simmons and Hoskins, 1978; 1980). Rossby wave dispersion is introduced by the meridional gradient of absolute ambient vorticity, so both by differential horizontal shear and the meridional derivative β of planetary vorticity f . The spherical shape of the Earth can introduce some buffering capacity of the absolute vorticity gradient to any modification by horizontal shear. A poleward shift of the storm track reduces the amount of Rossby wave dispersion experienced by baroclinic waves which would otherwise lead to barotropic conversion and a limiting of the modal growth rates. In that respect, the meridional shift of synoptic disturbances to higher latitudes might be buffering the effect of increased horizontal shear.

Some interesting context for our findings is provided by a number of studies that have investigated properties

FIGURE 4 Time-mean zonal-mean meridional eddy momentum flux (colour shading, $\text{m}^2 \cdot \text{s}^{-2}$) and meridional gradient of zonal-mean zonal velocity (contours) for different aquaplanet configurations. Solid (dashed) contours indicate a positive (negative) gradient with a contour spacing of $0.5 \text{ m} \cdot \text{s}^{-1} (\text{°N})^{-1}$ and the zero contour omitted



of the eddy-driven jet depending on its latitude. Specifically, Kidston and Vallis (2010) found a meridional shift of the jet's maximum in a baroclinic model similar to PUMA as the response to increased horizontal shear or reduced low-level baroclinicity. Kidston and Vallis (2010, 2012) explained the broadening and poleward shift as a consequence of reduced wave dissipation and increased barotropic instability at the poleward edge of a strengthened jet with stronger vorticity gradients. Barnes *et al.* (2010) found the development of a turning latitude and reduced wave breaking on the poleward side of a poleward shifted jet and analyzed the effect of an

inhibited eddy-mean flow feedback on jet persistence in a barotropic model. Here, Figure 4 shows how in PUMA the up-gradient meridional flux of zonal momentum on the poleward side of the jet is much weaker than on the equatorward side, very similar to the experiments by Barnes *et al.* (2010). In fact, there are signs of a down-gradient eddy momentum flux for the low-friction cases. It is evident in Figure 4 that, for friction time-scales $\tau_f > 2$ days, poleward eddy momentum flux reaches right to the poles when, concurrently, the storm track shown in Figure 3 is greatly extended on its poleward side. So, it could be concluded that the meridional shift of the poleward storm

track boundary for $\tau_f > 2$ days and the broadening of the jet seen in Figure 1 is caused by barotropic instability and that the onset of barotropic instability might be masking the effect of the governor in some places.

However, the main finding to be taken from Figure 4 is the reduction of eddy momentum flux convergence for an increasing surface friction time-scale τ_f . This is readily understood bearing in mind that the vertically integrated eddy momentum flux convergence maintains the barotropic jet against surface friction since the Coriolis force drops out in the vertical integral (e.g., Green, 1970). Specifically, the governing equation for zonally averaged zonal momentum in spherical, log-pressure coordinates where a , ρ_0 , and ϕ denote the earth radius, reference density, and latitude, respectively, and applying a Reynolds averaging to all velocity components with $u' = u - \bar{u}$, etc., where \bar{u} represents the zonal mean, is given by:

$$\frac{D\bar{u}}{Dt} - f\bar{v} = - (a \cos^2 \phi)^{-1} \left[\cos^2 \phi \overline{u'v'} \right]_{\phi} - \rho_0^{-1} \left[\rho_0 \overline{u'w'} \right]_z + \bar{X}, \quad (2)$$

$$\text{where } \frac{D\bar{u}}{Dt} = \bar{u}_t + \bar{v}(a \cos \phi)^{-1} (\bar{u} \cos \phi)_{\phi} + \bar{w} \bar{u}_z$$

is the material derivative of westerly momentum involving the advection by the Eulerian mean meridional overturning (\bar{v}, \bar{w}) and where the dissipative term \bar{X} is dominated by surface friction as given by Equation (1). Note that in the Eulerian mean, the convergence of the vertical flux of horizontal momentum is small, and that in steady state, the dominant balance is between surface friction, horizontal eddy-momentum flux convergence, and the Coriolis force $f\bar{v}$. In that respect, Equation (2) assists in understanding the weakening of the zonal-mean Ferrel cell seen in Figure 2 since less eddy-momentum flux convergence and less surface friction are balanced by a reduced Coriolis force associated with reduced equatorward mean flow in the upper troposphere and a reduced westward acceleration near the surface.

The Transformed Eulerian mean (TEM; Edmon *et al.*, 1980; Andrews *et al.*, 1987) defines residual (\bar{v}_*, \bar{w}_*) velocities with a residual circulation streamfunction (Figures 5 and 6) to take account of the mass transport by eddy motion in addition to the Eulerian mean overturning. In that framework, the zonally averaged zonal momentum equation is given by:

$$\frac{D\bar{u}}{Dt} - f\bar{v}_* = (\rho_0 a \cos \phi)^{-1} \nabla \cdot \bar{\mathbf{F}} + \bar{X}, \quad (3)$$

where $D\bar{u}/Dt$ is now the material derivative of westerly momentum involving the advection by the residual

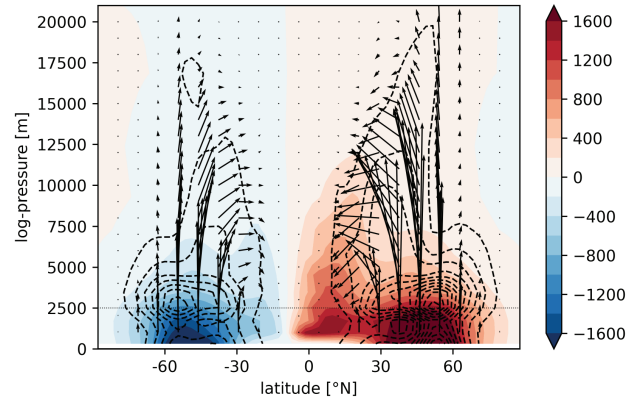


FIGURE 5 TEM residual mass streamfunction (colour shading, $\text{kg}\cdot\text{m}^{-1}\cdot\text{s}^{-1}$), mass weighted EP-flux divergence (black contours, $\text{m}^2\cdot\text{s}^{-2}$), and EP-flux vectors (arrows, scaled as recommended by Jucker (2021)) in spherical, log-pressure coordinates with scale height $H = 7,000$ m for the aquaplanet with $\tau_f = 1$ day. Dashed (solid) contours indicate EP-flux convergence (divergence) with a spacing of $25 \text{ m}^2 \cdot \text{s}^{-2}$; the horizontal dotted line indicates the top of the planetary boundary layer

circulation (\bar{v}_*, \bar{w}_*). The meridional and vertical components of the Eliassen–Palm (EP) flux $F^{(\phi)}$ and $F^{(z)}$ are given by:

$$F^{(\phi)} = \rho_0 a \cos \phi \left(\bar{u}_z \frac{\overline{v'\theta'}}{\bar{\theta}_z} - \overline{u'v'} \right), \quad (4)$$

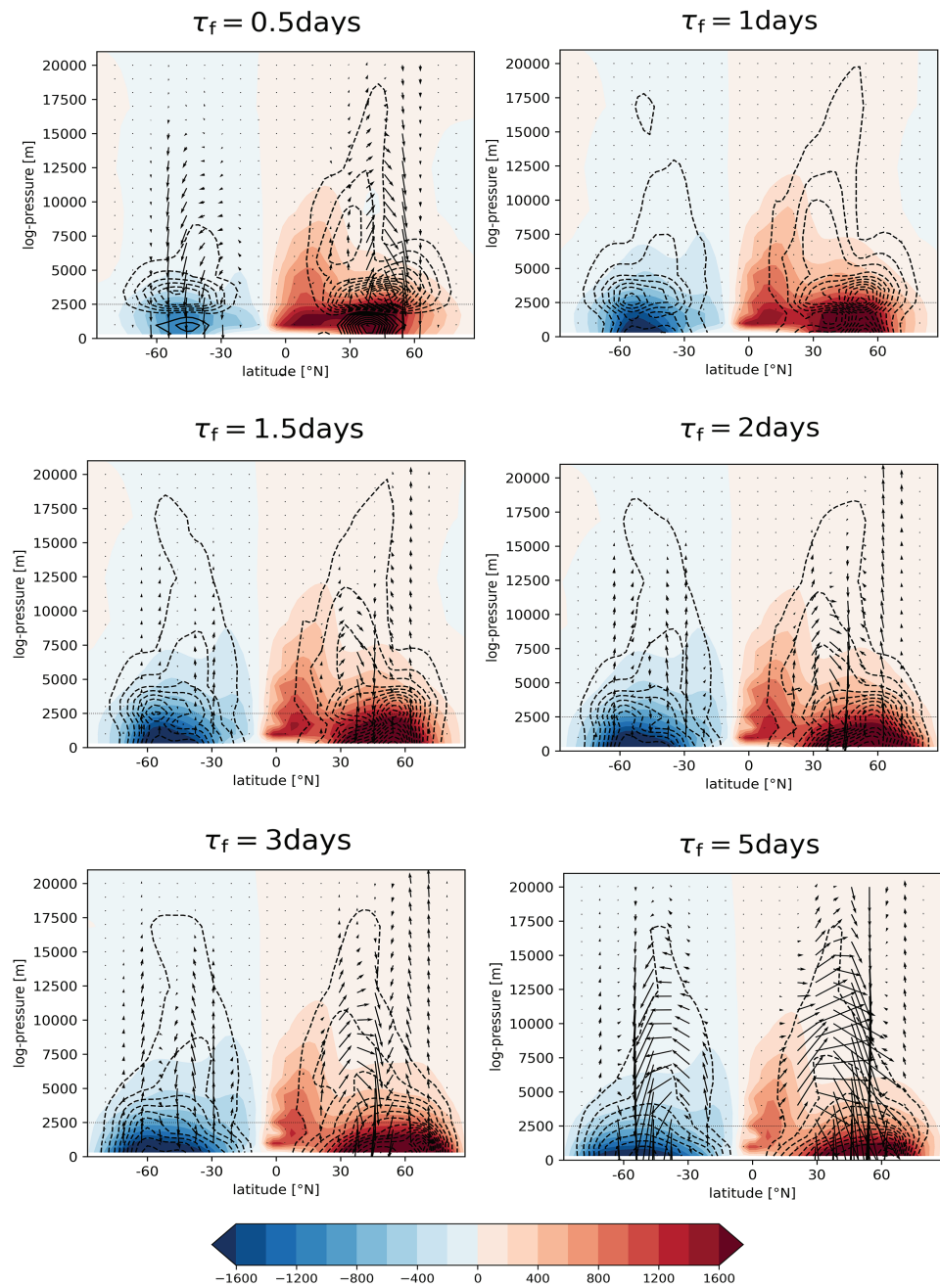
$F^{(z)} =$

$$\rho_0 a \cos \phi \left[- \left\{ (a \cos \phi)^{-1} (\cos \phi \bar{u})_{\phi} - f \right\} \frac{\overline{v'\theta'}}{\bar{\theta}_z} - \overline{u'w'} \right]. \quad (5)$$

In contrast to the Eulerian mean overturning, the residual circulation is composed of a single thermally direct cell in either hemisphere as displayed in Figure 5 for the aquaplanet experiment with $\tau_f = 1$ day (e.g., Karoly *et al.*, 1997). Additionally, that Figure shows the EP flux vectors and EP-flux divergence. From Equation (3), it is evident that, in the TEM sense, the EP flux acts similarly to a flux of easterly momentum, providing a source of easterly momentum in regions of EP-flux convergence and a source of westerly momentum in regions of EP-flux divergence. The vertical component is dominated by the term involving the meridional heat flux, and is strong in midlatitudes at low altitudes and, in the TEM sense, corresponds to a vertical flux of westerly momentum into the planetary boundary layer.² The horizontal component,

²The correspondence between a vertical flux of momentum and the heat flux term in the vertical component of the EP flux is commonly made in

FIGURE 6 As Figure 5, but for different aquaplanet configurations where arrows indicate EP-flux anomalies compared to $\tau_f = 1$ day



on the other hand, is dominated by the negative of the meridional momentum flux, is mostly directed equatorward, is strong especially at the equatorward flank of the upper-tropospheric jet, and indicates a flux of westerly momentum from the Subtropics into the eddy-driven jet. Note, furthermore, that for the present simulations the

the oceanographic literature, following on from Greatbatch and Lamb (1990) and Gent *et al.* (1995). The correspondence can be understood in terms of the thermal wind equation whereby a horizontal eddy heat flux acts to reduce meridional temperature gradients and hence geostrophic shear by thermal wind. Physically, the momentum is fluxed vertically by means of an eddy form drag.

TEM representation of the residual circulation in Figures 5 and 6 suffers from a poorly resolved lower boundary condition and the mass transport streamlines are in many cases not closed at the surface. Due to a free-slip boundary condition, the meridional eddy heat flux maximizes at the surface, resulting in an all-negative EP-flux divergence for the experiments with $\tau_f > 0.5$ day. A modified TEM formulation that takes account of the surface boundary conditions might resolve that problem (e.g., Held and Schneider, 1999). However, above the boundary layer the residual circulation in Figures 5 and 6 should be well approximated.

Figure 6 shows the TEM diagnostics for the six different aquaplanet configurations. It can be seen that, to a large extent, both the residual circulation and the EP-flux divergence are invariant to changing surface friction. In other words, the EP-flux response to changing surface friction is largely rotational and a change in horizontal eddy momentum flux convergence is accompanied by a corresponding change in the convergence of the vertical component of the EP flux. That is confirmed by the arrows in Figure 6 depicting the anomaly of mean EP-flux relative to the model simulation with $\tau_f = 1$ day. A dipole character of the vertical EP-flux anomaly indicates a meridional shift of maximum upward EP-flux associated with a meridional shift of the storm track. More importantly, the reduction of upward EP flux illustrates the fact that, at a higher friction time-scale, a reduced flux of westerly momentum by eddy form drag is required to oppose surface drag. Given its connection to the meridional eddy heat flux, the reduction in the vertical momentum flux is another signature of the governor because it is an indication that baroclinic instability is being suppressed. The invariance of the residual circulation suggests that the zonal-mean field of diabatic heating is unchanged. For the present model, this means that the zonal-mean temperature field is insensitive to surface friction, as found in our experiments and also by Robinson (1997).

3.2 | Sensitivity of persistence to changing surface friction

This study was motivated by the idea that an under-representation of the barotropic governor may contribute to a lack of persistence in models used for seasonal prediction, contributing to the so-called signal-to-noise paradox. After having investigated synoptic variability and the poleward shift of the storm track, we turn to the analysis of variability on longer time-scales. To show spectral power at a range of time-scales, Figure 7 displays periodograms of meridional velocity at 357 hPa averaged horizontally between 20°N and the North Pole with an area-weighted average. The envelopes around the solid lines indicate the 95% confidence intervals estimated using Welch's method with 500 overlapping groups and a Hanning window taper. The horizontal average over the large range of latitudes is applied to account for any meridional shift of variability; this can be seen, for example, in Figure 3.

The estimates of power spectral density in Figure 7 show a clear dependency on surface friction and a distinct separation between the friction time-scales $\tau_f \leq 2$ days and $\tau_f \geq 3$ days which might be caused by the onset

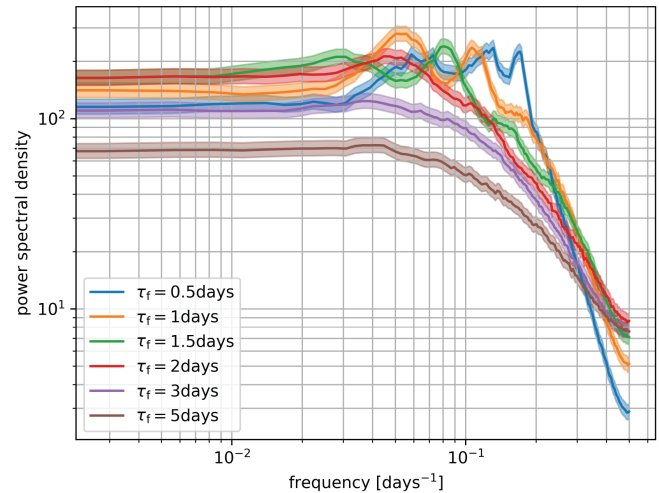


FIGURE 7 Area-weighted horizontal average of power spectral density ($\text{m}^2 \cdot \text{s}^{-2}$) of meridional velocity between 20°N and 90°N at 357 hPa for different aquaplanet configurations. The envelopes indicate the 95% confidence intervals assuming a χ^2 distribution with $500 \times 32/19$ degrees of freedom

of barotropic instability. Apart from the very high frequencies where strong friction damps variability, the dependency on surface friction might be summarized as a reduction of the overall level of noise with increasing friction time-scales. Whereas the low friction cases follow a fairly smooth curve resembling a red noise process with the highest power at low frequencies, the strong friction cases have maximum power at intermediate time-scales. Regarding the persistence of anomalies, it is interesting to take a closer look at the frequencies of these peaks in variance for the model runs with friction time-scales $\tau_f \leq 2$ days. Specifically, a local maximum of power spectral density can be seen at a period of approximately 6 days for the model run with $\tau_f = 0.5$ day. When surface friction is reduced, this first maximum of spectral power moves to longer periods up to around 20 days. In other words, reducing surface friction increases persistence at sub-seasonal time-scales; this is the most important finding of this study. Following the reasoning of Strommen and Palmer (2019), it follows that reducing the magnitude of surface friction has the potential to increase the signal-to-noise ratio at seasonal and decadal time-scales. Figure 7 also illustrates the role of the eddy feedback since, at very low frequencies, the maximum power occurs at intermediate friction time-scales despite the increasing role of the governor and the decreasing strength of the storm track as friction time-scales increase.

For a deeper insight into low-frequency variability, we now discuss the ensemble mean and ensemble spread of 90-day means processed from the tropical heating experiments. Section 2 gives information about how the time

series are resampled into 90-day means. Each of these samples can be regarded as an independent seasonal forecast for the teleconnections of a tropical anomaly. As expected from linear theory, the upper-tropospheric divergence associated with the idealized heating anomaly produces a Rossby wave train response which is baroclinic up to 20°N and equivalent barotropic from there on (e.g., Hoskins and Karoly, 1981). In the context of seasonal prediction, this will be considered the predictable signal which should be detectable in each forecast, that is, in each 90-day mean, but is best represented by the ensemble mean.

In order to estimate the stationary wave response, long-time mean horizontal streamfunction perturbations are computed for the two independent ensembles of 90-day means. The difference between the two ensembles (not shown) is small relative to the contour spacing in Figure 8, supporting the statistical significance of our results. Subtracting the long-term zonal mean removes any zonal mean effect of the tropical heating which does modify the zonal mean thermal structure, but is also limiting the informative value in perturbations close to the pole. Note that horizontal streamfunction is calculated at 357 hPa, however the signal is equivalent barotropic in the plotted domain north of 20°N .

The north polar stereographic plots (Figure 8) indicate different ray paths depending on surface friction. From linear theory, we can expect that, starting in the Tropics, long zonal wavelengths will propagate northward across the pole whereas short zonal wavelengths get reflected at a turning latitude associated with the poleward flank of the jet (e.g., Hoskins and Karoly, 1981). By changing the basic state jet, reduced surface friction will consequently modify the ray path. Indeed, for strong friction we see zonally elongated signals, and for weak friction a more meridional propagation. When the mean jet is extended right to the pole for friction time scales $\tau_f \geq 3$ days, the ray paths clearly traverse the North Pole. On the other hand, Hoerling and Ting (1994) have demonstrated the importance of extratropical transients in producing the stationary wave response to a tropical heating anomaly, which constitutes an additional mechanism by which the barotropic governor can influence the extratropical signal aside from changing the basic state. In addition to a modified ray path, the intensity of the ensemble mean signal is substantially enhanced for reduced friction, a result especially relevant for the signal-to-noise ratio.³

As well as the ensemble mean signal, we are interested in the ensemble spread between individual 90-day

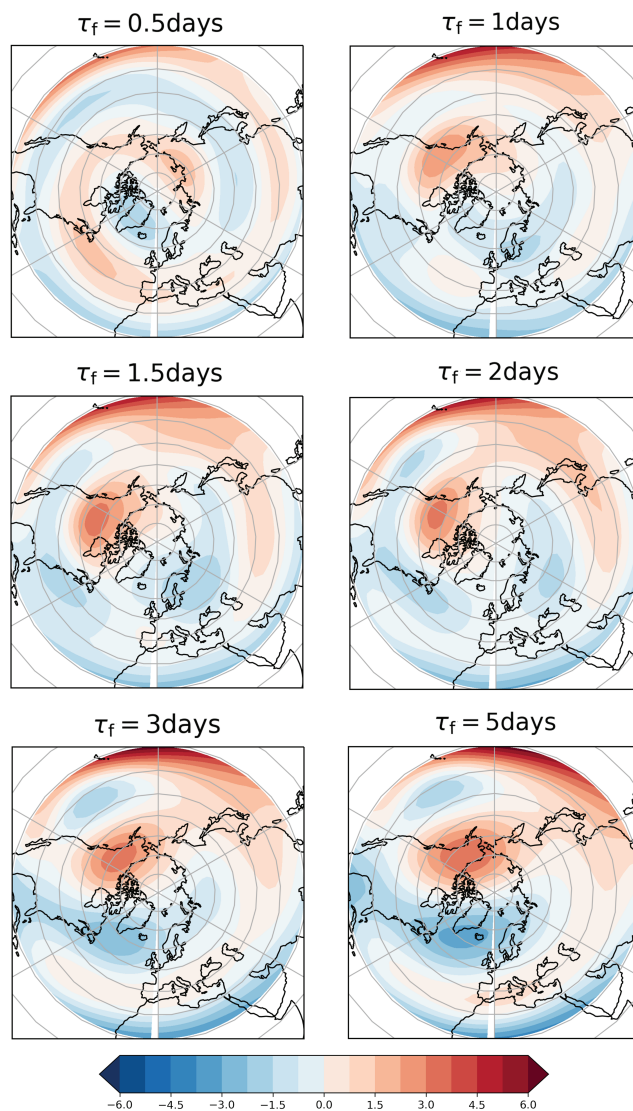


FIGURE 8 Ensemble mean streamfunction perturbations ($10^6 \text{m}^2 \cdot \text{s}^{-1}$) from the time-mean zonal mean at 357 hPa between 20°N and 90°N for different configurations of the experiments with tropical heating anomaly. The plotted coastlines are close to meaningless since the extratropical set-up is still zonally symmetric and is only meant to provide guidance for comparison with known modes of variability such as ENSO

periods of the long time series. Therefore, Figure 9 shows the zonal-mean standard deviation of 90-day mean streamfunction perturbations at 357 hPa, although it can be noted that in the Extratropics these perturbations are equivalent barotropic. Overall, there is little spread in the Tropics but a much larger spread in the Extratropics. Depending on surface friction, there are two to three local maxima in either hemisphere. For friction time-scales $\tau_f \geq 3$ days, the local maxima are less pronounced and the overall level of noise is reduced. Consequently, we see a larger signal-to-noise ratio for reduced surface friction

³Explicit plots of the signal-to-noise ratio and a discussion of its connection to the ratio of predictable components (RCP), are given in Supporting Information Appendix S2 and Figure S4.

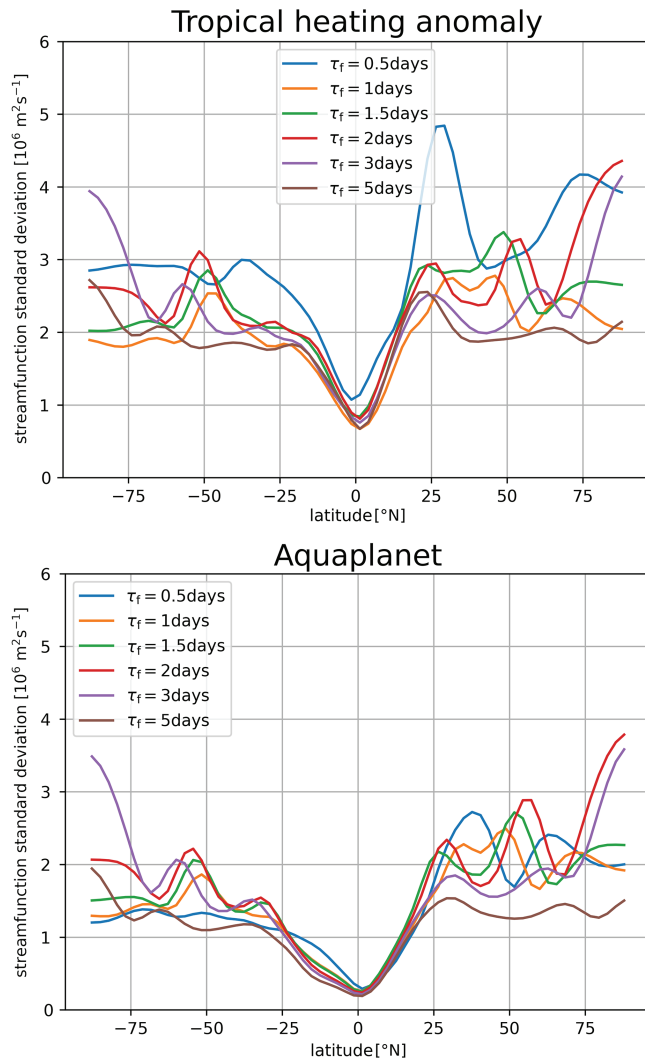


FIGURE 9 Zonal-mean standard deviation of 90-day mean streamfunction perturbations (ensemble spread) at 357 hPa from the time-mean zonal mean for different model configuration

(Figure S4). For friction time-scales $\tau_f < 3$ days, the reduction in spread is less clear, similarly to what is found for total variance of zonal momentum (Figures 1 and S1). The principal difference between experiments with that range of friction time-scales is a poleward shift of the local maxima as friction is reduced. A third maximum develops in the Subtropics when the other two maxima have moved sufficiently. This shift is similar to and likely associated with the movement of the storm track (Section 3.1). Given that similarity, it is tempting to connect the maxima of observed spread between 90-day means with the mechanism of the NAO. Vallis *et al.* (2004) present a mechanism where the typical circulation dipole pattern of low-frequency variability is created by a monopole vorticity flux anomaly which is reminiscent of the present model results where temporal variations in storm track intensity represent monopole vorticity flux anomalies. However,

this mechanism is not sufficient to explain the whole picture in Figure 9 since there are considerable differences between the experiments with and without a tropical heating anomaly, especially in the region of the subtropical jet. Understanding the interactions between a stationary Rossby wave train and internal extratropical variability clearly requires further analyses.

4 | DISCUSSION

Changing surface friction has a profound influence on the general circulation in a simplified atmospheric model. At reduced friction, the barotropic component of the westerly jets is strengthened and the Ferrel cell overturning weakened. Moreover, this study confirms the finding of a barotropic governor by James and Gray (1986) and James (1987): the increased horizontal shear in response to reduced friction suppresses synoptic variability in the form of baroclinic instability. Specifically, the governor acts in a way that the EP-flux response to a modified friction parameter is largely rotational and the residual circulation preserved. It means that any change in horizontal momentum flux convergence needed to maintain the barotropic jet against surface friction and to balance the Eulerian mean overturning is accompanied by a change in eddy heat flux. The suppression of baroclinic instability is associated with a poleward shift of the storm track, although the effects of the governor might to some extent be masked by the onset of barotropic instability on the poleward side of the jet as the jet strength increases.

The reduction of eddy fluxes associated with baroclinic instability has important consequences for atmospheric variability. In consequence of the suppression of baroclinic instability, it is found that the preferred time-scale of sub-seasonal variability lengthens, that is, persistence is increased. On longer time-scales, variability maximizes for intermediate friction parameters before barotropic instability takes over. By emulating ensemble forecasts as 90-day means of a stationary Rossby wave train, it is shown how surface friction can influence the signal-to-noise ratio. Specifically, reduced surface friction alters the spatial distribution of variance, reduces the ensemble spread in seasonal forecasts, and strengthens the ensemble mean by enhancing the signal.

These idealized experiments suggest that mistuned parameters controlling mechanical damping, and possibly also form drag or gravity wave drag, might cause the persistence bias or signal-to-noise paradox seen in sophisticated climate prediction systems (e.g., Athanasiadis *et al.*, 2017; Baker *et al.*, 2018). Admittedly, the idealized model and experimental design have limitations. For example, it could be argued that some characteristics of the

signal-to-noise paradox, such as a realistic level of overall variance (Scaife and Smith, 2018), are not captured by the simplified model. Also, if the barotropic governor is, indeed, not operating correctly in sophisticated climate prediction systems, then correcting it might exacerbate present biases like underestimated eddy momentum flux convergence and a poleward shifted jet in the North Atlantic region (Scaife *et al.*, 2019). However, the demonstration of the role that can be played by the barotropic governor as presented by this study has to be seen as a proof of concept and might be concealed in more complex models by tuning multiple parameters. Specifically, this simple model shows that, instead of an underestimated sensitivity of the model to tropical teleconnections or other predictable components of the climate system, adiabatic extratropical dynamics could prove responsible for underestimating the signal compared to the noise in seasonal predictions and hence could be of importance for the signal-to-noise paradox.

Finally, the governor concept appears to be of more general significance than the connection between surface friction and baroclinic instability. When James and Gray (1986) identified the barotropic governor, they found that dissipation of mean flow kinetic energy affects the conversion of available potential energy (APE) to eddy-kinetic energy (EKE). Ma *et al.* (2016) find an oceanic governor mechanism that involves atmosphere–ocean coupling. Specifically, it is found that suppressed dissipation of eddy APE in the Kuroshio Extension region suppresses baroclinic instability and prevents the establishment of the Kuroshio Extension jet in two coupled climate models. Another governor mechanism appears to control barotropic instability of the upper-tropospheric rotational flow since that is found to be much more unstable in a two-dimensional model than in reality (Wicker, 2020), leading to the concept of the *baroclinic governor* as noted by Mak (2011). In the coming years, it will be interesting to see whether the coupling of the various climate system components in modern Earth System models will reveal more examples of a governor of dynamic instability.

AUTHOR CONTRIBUTIONS


Wolfgang Wicker: conceptualization; investigation; writing – original draft. **Richard J. Greatbatch:** conceptualization; writing – review and editing. **Martin Claus:** methodology; writing – review and editing.

ACKNOWLEDGEMENTS

The authors are grateful to those at the Meteorological Institute of the University of Hamburg who developed the Portable University Model of the Atmosphere (PUMA).

We also appreciate the help of two anonymous reviewers whose comments led to significant improvement of this manuscript. WW is grateful for six months' support from GEOMAR which enabled this work to be completed.

ORCID

Wolfgang Wicker  <https://orcid.org/0000-0002-8951-2875>

Richard J. Greatbatch  <https://orcid.org/0000-0001-5758-2249>

Martin Claus  <https://orcid.org/0000-0002-7525-5134>

REFERENCES

- Andrews, D.G., Holton, J.R. and Leovy, C.B. (1987) *Middle Atmosphere Dynamics*. Cambridge, MA: Academic Press.
- Athanasiadis, P.J., Bellucci, A., Scaife, A.A., Hermanson, L., Materia, S., Sanna, A., Borrelli, A., MacLachlan, C. and Gualdi, S. (2017) A multisystem view of wintertime NAO seasonal predictions. *Journal of Climate*, 30, 1461–1475.
- Baker, L., Shaffrey, L., Sutton, R., Weisheimer, A. and Scaife, A.A. (2018) An inter-comparison of skill and overconfidence/underconfidence of the wintertime North Atlantic Oscillation in multimodel seasonal forecasts. *Geophysical Research Letters*, 45, 7808–7817.
- Barnes, E.A., Hartmann, D.L., Frierson, D.M. and Kidston, J. (2010) Effect of latitude on the persistence of eddy-driven jets. *Geophysical Research Letters*, 37(11). <https://doi.org/10.1029/2010GL043199>.
- Cai, M. and van den Dool, H.M. (1991) Low-frequency waves and traveling storm tracks. Part I: Barotropic component. *Journal of Atmospheric Sciences*, 48, 1420–1436.
- Charney, J. (1947) The dynamics of long waves in a westerly baroclinic current. *Journal of Meteorology*, 4, 135–163.
- Chen, G., Held, I.M. and Robinson, W.A. (2007) Sensitivity of the latitude of the surface westerlies to surface friction. *Journal of the Atmospheric Sciences*, 64, 2899–2915.
- Dunstone, N.J., Smith, D., Scaife, A.A., Hermanson, L., Eade, R., Robinson, N., Andrews, M. and Knight, J. (2016) Skilful predictions of the winter North Atlantic Oscillation one year ahead. *Nature Geoscience*, 9, 809–814.
- Eade, R., Smith, D., Scaife, A.A., Wallace, E., Dunstone, N.J., Hermanson, L. and Robinson, N. (2014) Do seasonal-to-decadal climate predictions underestimate the predictability of the real world?. *Geophysical Research Letters*, 41, 5620–5628.
- Eady, E.T. (1949) Long waves and cyclone waves. *Tellus*, 1, 33–52.
- Edmon, H.J., Hoskins, B.J. and McIntyre, M.E. (1980) Eliassen–Palm cross-sections for the troposphere. *Journal of Atmospheric Sciences*, 37, 2600–2616.
- Fraedrich, K., Kirk, E. and Lunkeit, F. (1998). *PUMA: Portable University Model of the Atmosphere*. DKRZ Technical Report 16, Meteorologisches Institut Hamburg, Germany.
- Fraedrich, K., Kirk, E., Luksch, U. and Lunkeit, F. (2005) The Portable University Model of the Atmosphere (PUMA): storm-track dynamics and low-frequency variability. *Meteorologische Zeitschrift*, 14, 735–745. <https://doi.org/10.1127/0941-2948/2005/0074>.

- Gent, P.R., Willebrand, J., McDougall, T.J. and McWilliams, J.C. (1995) Parameterizing eddy-induced tracer transports in ocean circulation models. *Journal of Physical Oceanography*, 25, 463–474.
- Gollan, G., Bastin, S. and Greatbatch, R.J. (2019) Tropical precipitation influencing boreal winter midlatitude blocking. *Atmospheric Science Letters*, 20(5). <https://doi.org/10.1002/asl.900>.
- Greatbatch, R.J. and Lamb, K.G. (1990) On parameterizing vertical mixing of momentum in non-eddy-resolving ocean models. *Journal of Physical Oceanography*, 20, 1634–1637.
- Green, J.S.A. (1970) Transfer properties of the large-scale eddies and the general circulation of the atmosphere. *Quarterly Journal of the Royal Meteorological Society*, 96, 157–185.
- Hardiman, S.C., Dunstone, N.J., Scaife, A.A., Smith, D.M., Knight, J.R., Davies, P., Claus, M. and Greatbatch, R.J. (2020) Predictability of European winter 2019/2020: Indian Ocean dipole impacts on the NAO. *Atmospheric Science Letters*, 21, e1005.
- Held, I.M. and Schneider, T. (1999) The surface branch of the zonally averaged mass transport circulation in the troposphere. *Journal of the Atmospheric Sciences*, 56, 1688–1697.
- Hoerling, M.P. and Ting, M. (1994) Organization of extratropical transients during El Niño. *Journal of Climate*, 7, 745–766.
- Horel, J.D. and Wallace, J.M. (1981) Planetary-scale atmospheric phenomena associated with the Southern Oscillation. *Monthly Weather Review*, 109, 813–829.
- Hoskins, B.J. and Karoly, D.J. (1981) The steady linear response of a spherical atmosphere to thermal and orographic forcing. *Journal of the Atmospheric Sciences*, 38, 1179–1196.
- Hoskins, B.J. and Simmons, A. (1975) A multi-layer spectral model and the semi-implicit method. *Quarterly Journal of the Royal Meteorological Society*, 101, 637–655.
- James, I.N. (1987) Suppression of baroclinic instability in horizontally sheared flows. *Journal of the Atmospheric Sciences*, 44, 3710–3720.
- James, I.N. and Gray, L.J. (1986) Concerning the effect of surface drag on the circulation of a baroclinic planetary atmosphere. *Quarterly Journal of the Royal Meteorological Society*, 112, 1231–1250.
- James, I.N. and James, P.M. (1989) Ultra-low-frequency variability in a simple atmospheric circulation model. *Nature*, 342, 53–55.
- Jucker, M. (2021) Scaling of Eliassen–Palm flux vectors. *Atmospheric Science Letters*, 22, e1020.
- Karoly, D.J., McIntosh, P.C., Berrisford, P., McDougall, T. and Hirst, A.C. (1997) Similarities of the Deacon cell in the southern ocean and Ferrel cells in the atmosphere. *Quarterly Journal of the Royal Meteorological Society*, 123, 519–526.
- Kidston, J. and Vallis, G.K. (2010) Relationship between eddy-driven jet latitude and width. *Geophysical Research Letters*, 37. <https://doi.org/10.1029/2010GL044849>.
- Kidston, J. and Vallis, G.K. (2012) The relationship between the speed and the latitude of an eddy-driven jet in a stirred barotropic model. *Journal of the Atmospheric Sciences*, 69, 3251–3263.
- Kunz, T., Fraedrich, K. and Lunkeit, F. (2009) Synoptic-scale wave breaking and its potential to drive NAO-like circulation dipoles: a simplified GCM approach. *Quarterly Journal of the Royal Meteorological Society*, 135, 1–19.
- Latif, M., Anderson, D., Barnett, T., Cane, M., Kleeman, R., Leetmaa, A., O'Brien, J., Rosati, A. and Schneider, E. (1998) A review of the predictability and prediction of ENSO. *Journal of Geophysical Research: Oceans*, 103, 14375–14393.
- Lorenz, D.J. and Hartmann, D.L. (2003) Eddy–zonal flow feedback in the Northern Hemisphere winter. *Journal of Climate*, 16, 1212–1227.
- Lorenz, E.N. (1955) Available potential energy and the maintenance of the general circulation. *Tellus*, 7, 157–167.
- Lorenz, E.N. (1963) Deterministic nonperiodic flow. *Journal of Atmospheric Sciences*, 20, 130–141.
- Ma, X., Jing, Z., Chang, P., Liu, X., Montuoro, R., Small, R.J., Bryan, F.O., Greatbatch, R.J., Brandt, P., Wu, D., Lin, X. and Wu, L. (2016) Western boundary currents regulated by interaction between ocean eddies and the atmosphere. *Nature*, 535, 533–537.
- Mak, M. (2011) *Atmospheric Dynamics*. Cambridge, UK: Cambridge University Press.
- O'Reilly, C.H., Woollings, T., Zanna, L. and Weisheimer, A. (2018) The impact of tropical precipitation on summertime Euro-Atlantic circulation via a circumglobal wave train. *Journal of Climate*, 31, 6481–6504.
- O'Reilly, C.H., Weisheimer, A., Woollings, T., Gray, L.J. and MacLeod, D. (2019) The importance of stratospheric initial conditions for winter North Atlantic Oscillation predictability and implications for the signal-to-noise paradox. *Quarterly Journal of the Royal Meteorological Society*, 145, 131–146.
- Robinson, W.A. (1997) Dissipation dependence of the jet latitude. *Journal of Climate*, 10, 176–182.
- Scaife, A.A. and Smith, D. (2018) A signal-to-noise paradox in climate science. *NPJ Climate and Atmospheric Science*, 1, 1–8.
- Scaife, A.A., Arribas, A., Blockley, E., Brookshaw, A., Clark, R., Dunstone, N.J., Eade, R., Fereday, D., Folland, C.K., Gordon, M., Hermanson, L., Knight, J.R., Lea, D.J., MacLachlan, C., Maidens, A., Martin, M., Peterson, A.K., Smith, D., Vellinga, M., Wallace, E., Waters, J. and Williams, A. (2014) Skillful long-range prediction of European and North American winters. *Geophysical Research Letters*, 41, 2514–2519.
- Scaife, A.A., Comer, R.E., Dunstone, N.J., Knight, J.R., Smith, D.M., MacLachlan, C., Martin, N., Peterson, K.A., Rowlands, D., Carroll, E.B., Belcher, S.E. and Slingo, J.M. (2017) Tropical rainfall, Rossby waves and regional winter climate predictions. *Quarterly Journal of the Royal Meteorological Society*, 143, 1–11.
- Scaife, A.A., Camp, J., Comer, R., Davis, P., Dunstone, N.J., Gordon, M., MacLachlan, C., Martin, N., Nie, Y., Ren, H.-L., Roberts, M., Robinson, W., Smith, D. and Vidale, P.L. (2019) Does increased atmospheric resolution improve seasonal climate predictions?. *Atmospheric Science Letters*, 20. <https://doi.org/10.1002/asl.922>.
- Scinocca, J. and Haynes, P. (1998) Dynamical forcing of stratospheric planetary waves by tropospheric baroclinic eddies. *Journal of the Atmospheric Sciences*, 55, 2361–2392.
- Siegert, S., Stephenson, D.B., Sansom, P.G., Scaife, A.A., Eade, R. and Arribas, A. (2016) A Bayesian framework for verification and recalibration of ensemble forecasts: how uncertain is NAO predictability?. *Journal of Climate*, 29, 995–1012.
- Simmons, A.J. and Hoskins, B.J. (1978) The life cycles of some nonlinear baroclinic waves. *Journal of the Atmospheric Sciences*, 35, 414–432.
- Simmons, A.J. and Hoskins, B.J. (1980) Barotropic influences on the growth and decay of nonlinear baroclinic waves. *Journal of the Atmospheric Sciences*, 37, 1679–1684.
- Smith, D.M., Scaife, A.A. and Kirtman, B.P. (2012) What is the current state of scientific knowledge with regard to seasonal and

- decadal forecasting?. *Environmental Research Letters*, 7. <https://doi.org/10.1088/1748-9326/7/1/015602>.
- Stephenson, D.B. (1994) The Northern Hemisphere tropospheric response to changes in the gravity-wave drag scheme in a perpetual January GCM. *Quarterly Journal of the Royal Meteorological Society*, 120, 699–712.
- Strommen, K. and Palmer, T.N. (2019) Signal and noise in regime systems: a hypothesis on the predictability of the North Atlantic Oscillation. *Quarterly Journal of the Royal Meteorological Society*, 145, 147–163.
- Vallis, G.K., Gerber, E.P., Kushner, P.J. and Cash, B.A. (2004) A mechanism and simple dynamical model of the North Atlantic Oscillation and annular modes. *Journal of the Atmospheric Sciences*, 61, 264–280.
- Wicker, W. (2020). Modelling the upper-tropospheric rotational flow. Master's thesis.
- Wulff, C.O., Greatbatch, R.J., Domeisen, D.I., Gollan, G. and Hansen, F. (2017) Tropical forcing of the summer East Atlantic pattern. *Geophysical Research Letters*, 44, 11–166.
- Zhang, W. and Kirtman, B. (2019) Understanding the signal-to-noise paradox with a simple Markov model. *Geophysical Research Letters*, 46, 13308–13317.

SUPPORTING INFORMATION

Additional supporting information may be found online in the Supporting Information section at the end of this article.

How to cite this article: Wicker, W., Greatbatch, R.J. & Claus, M. (2022) Sensitivity of a simple atmospheric model to changing surface friction with implications for seasonal prediction. *Quarterly Journal of the Royal Meteorological Society*, 148(742), 199–213. Available from: <https://doi.org/10.1002/qj.4200>